Fine-tuning of colloidal polymer crystals by molecular simulation

Miguel Herranz, Clara Pedrosa, Daniel Martínez-Fernández, Katerina Foteinopoulou, Nikos Ch. Karayiannis, and Manuel Laso*

Institute for Optoelectronic Systems and Microtechnology (ISOM) and Escuela Técnica Superior de Ingenieros Industriales (ETSII), Universidad Politécnica de Madrid (UPM) C. José Gutiérrez Abascal 2, 28006 Madrid, Spain

(Received 21 June 2022; accepted 4 June 2023; published 21 June 2023)

Through extensive molecular simulations we determine a phase diagram of attractive, fully flexible polymer chains in two and three dimensions. A rich collection of distinct crystal morphologies appear, which can be finely tuned through the range of attraction. In three dimensions these include the face-centered cubic, hexagonal close packed, simple hexagonal, and body-centered cubic crystals and the Frank-Kasper phase. In two dimensions the dominant structures are the triangular and square crystals. A simple geometric model is proposed, based on the concept of cumulative neighbors of ideal crystals, which can accurately predict most of the observed structures and the corresponding transitions. The attraction range can thus be considered as an adjustable parameter for the design of colloidal polymer crystals with tailored morphologies.

DOI: 10.1103/PhysRevE.107.064605

I. INTRODUCTION

Crystallization is one of the most intriguing physicochemical processes in science and technology. While of paramount importance in materials design and engineering, key aspects of the phenomenon remain rather poorly understood. Thus, it is imperative to establish a connection between behavior at the level of atoms and molecules, the ensuing ordered structures, and eventually the macroscopic properties of the end material.

Very recently through the emergence of "digital alchemy" [1] the concept has been tackled through a new perspective: one starts from the target morphologies and searches, mainly through computational tools, for the molecular shape and size that would produce them [2]. Such reverse engineering methods, combined with robust algorithms, machine learning, and predictive modeling have led to significant advances in the computer-aided design of soft materials made of self-assembled colloids and nanoparticles [3,4]. As an alternative, the shape and size of hard-body objects can be effectively replaced by fine tuning the pairwise interactions between the species, be they particles or atoms, in order to achieve the desired geometric patterns [5–7]. These simulation breakthroughs have been accompanied by vigorous progress in colloidal synthesis allowing for a systematic, instead of trial-and-error, fabrication of optimal structures based on self-organization from properly selected building blocks [8–13].

The phase behavior of macromolecular systems is equally important [14] and more complex compared to the one of monomeric analogs due to the wide spectrum of characteristic length and time scales involved. Designing crystals made of soft or hard colloidal polymers and molecules [15,16] remains a formidable challenge in spite of the important experimental [17–23] and modeling [24–28] advances in synthesis, characterization, and property prediction.

In the present contribution we demonstrate a hierarchical modeling approach for the design and morphological fine tuning of crystals of colloidal polymers with short-range attractive interactions. First, we describe the macromolecular system at hand, then we introduce a geometric neighbor model to predict the thermodynamically stable crystal, and finally we resort to simulations to verify and extend analytical predictions.

II. MODEL, SYSTEMS, AND METHODOLOGY

A. Molecular model

The colloidal polymer model we have chosen (in two and three dimensions) is a bulk assembly of linear, freely jointed chains of tangent, nonoverlapping spheres of uniform diameter σ_1, which is further the characteristic unit length of the system, taken here as unity. Bonded monomers along the chain backbone are tangent within a numerical tolerance of $dl = 6.5 \times 10^{-4}$. Practically, this means that no gaps exist between bonded sites. Such gaps are known to profoundly affect the phase behavior of chains and the ensuing crystal morphologies [29,30]. Short-range, pairwise attraction is realized through the square well (SW) potential, described by

$$u_{SW}(r_{ij}) = \begin{cases} 0, & r_{ij} \geqslant \sigma_2 \\ -\epsilon, & \sigma_1 \leqslant r_{ij} < \sigma_2 \\ \infty, & r_{ij} < \sigma_1 \end{cases}, \tag{1}$$

where the tunable parameters correspond to the intensity (depth) ϵ and the range of interaction σ_2, the latter being expressed in units of σ_1 ($\sigma_2 > \sigma_1$). In Eq. (1) $u_{SW}(r_{ij})$ is the energy that corresponds to the interaction of two monomers i and j whose centers lie at a distance r_{ij}.

*n.karayiannis@upm.es; manuel.laso@upm.es

Since the early works of Young and Alder [31,32], the SW model has been applied to study (free) energy-driven processes in monomeric and more complex systems, and has provided insights into the phase behavior, coalescence, and percolation of monomers [33–41], and protein folding and self-assembly of single chains [42–46].

B. Geometric neighbor model

The proposed geometric neighbor model is particularly simple, and it follows a concept similar to the one proposed by Serrano-Illán *et al*. as analyzed in [39]. Given the entirely attractive nature of the interactions, thermodynamic stability of the crystals is primarily dictated by the number of neighbors as a function of distance. The more neighbors packed within a radius equal to the attraction range σ_2, the lower the potential energy and (ignoring entropic differences among polymorphs, which are known to be quite small [47–51]) the more stable the corresponding crystal.

The tangency condition imposed by chain connectivity in fact simplifies the analysis of polymeric analogs: first, because only strictly tangent polymer crystals have to be considered and, second, with respect to simulations, the bonds along the chain backbone stabilize cluster formation compared to monomeric analogs for the same attraction intensity.

The following crystals have been considered for the geometric neighbor model: honeycomb (HON), square (SQU), and triangular (TRI) 2D crystals, and the face-centered cubic (FCC), hexagonal close packed (HCP), holoedric 6/mmm (simple hexagonal or HEX), and body-centered cubic (BCC) 3D crystals, whose structures and properties can be found in [52].

Figure 1 shows the number of neighbors as a function of distance for the above crystal types in two dimensions (top panel) and three dimensions (bottom panel). Starting with two dimensions, the geometric model predicts that the TRI crystal is the prevailing one from the point of view of energy in all ranges except the intervals $1.41 \leqslant r \leqslant 1.73$ (Region B) and $2.24 \leqslant r \leqslant 2.65$ (Region E) where a site in the SQU crystal has more neighbors within a circle of diameter σ_2. The HON is systematically more dilute and thus the least stable crystal in the whole attraction range.

In the 3D case, six distinct regions can be identified. The initial dominance of HCP/FCC (Region I) is succeeded by BCC (Region II), HEX (Region III), again BCC (Region IV), FCC (Region V), and HCP/BCC (Region VI). At first glance it is unexpected that for distances in the range of $1.15 \leqslant r \leqslant 1.73$ the noncompact HEX and BCC crystals prevail. Still, the dominance of noncompact crystals, as calculated here, is in agreement with the density-based calculations in Ref. [39].

The phase diagram of Fig. 1, as predicted by the geometric neighbor model, raises a number of intriguing questions, especially whether the expected ordered morphologies can appear "in reality." We remind readers here that any entropic contributions, both translational and conformational, are ignored. Information in the geometric neighbor model about chain connectivity is solely incorporated through the tangency condition, effectively enforcing the absence of gaps between the interlattice sites. Thus, this straightforward geometric argument can be considered as only a first-order approximation (but a successful one, as will be shown below).

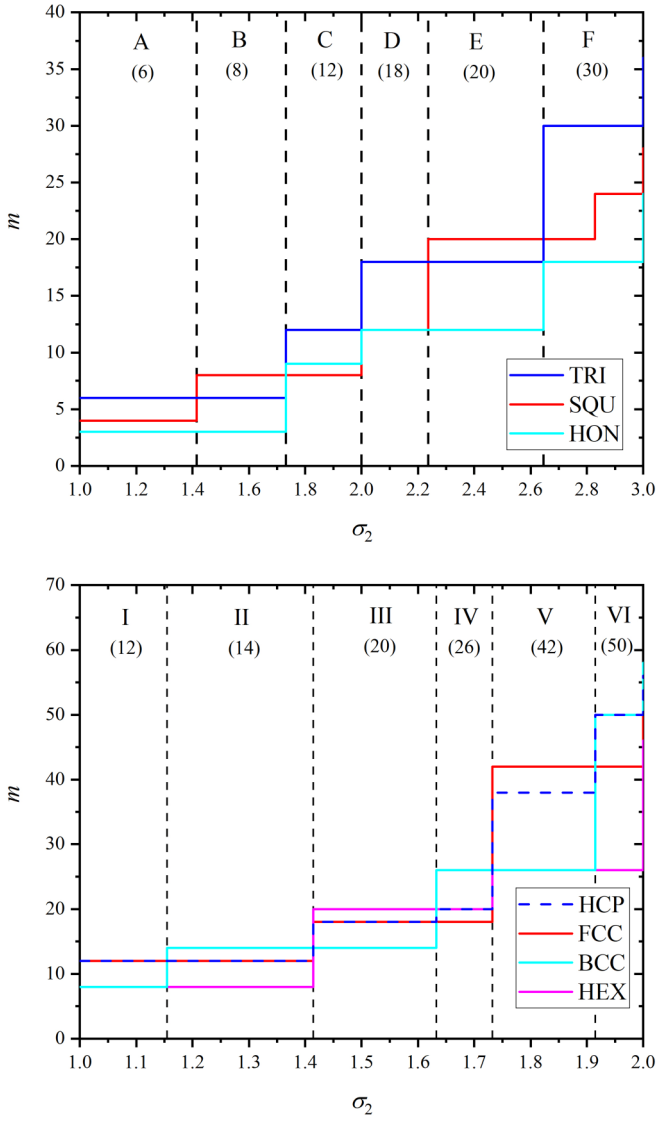

FIG. 1. Number of neighbors, m, as a function of distance from a reference site, σ_2, for (bottom panel) the HCP, FCC, BCC, and HEX crystals in three dimensions and (top panel) the TRI, SQU, and HON crystals in two dimensions. Dashed vertical lines identify the values at which the steps take place. Each region is identified by a roman number (3D) or letter (2D). Arabic numbers in parentheses correspond to the cumulative number of neighbors for the most stable crystal in the given region.

C. Monte Carlo simulations

To validate the predictive capacity of the proposed model, we carry out extensive simulations for the generation and equilibration of the systems composed of 100 attractive chains of average chain length $N_{av} = 12$ for a total of $N = 1200$ interacting sites. Regarding the simulations and the successive structural identification of the generated system configurations, we employ Simu-D, a home-made simulator-descriptor software suite [53]. The simulator component is a Monte Carlo (MC) protocol based on local, cluster

and chain-connectivity-altering moves (CCAMs) [54–56] as in all our recent works on (free) energy-driven [57] and athermal [58–60] polymer-based systems. The MC mix is composed of (1) rotation (10%), (2) reptation (10%), (3) flip (34.7%), (4) intermolecular reptation (25%), (5) configurational bias (20%), (6) simplified end bridging (0.1%), and (7) simplified intermolecular end-bridging (0.1%) and cluster moves (0.1%) where numbers in parentheses correspond to attempt percentages. Furthermore, a cluster analysis is attempted at regular intervals (10^7 steps) to disable cluster moves when there is just one cluster or (re)activate them in the opposite case. Clusters are detected using an approach similar to the DBSCAN algorithm [61,62], where the distance criterion is set to 1.2 (in units of σ_1). As explained in detail in [53,55,56] every local MC move is executed in a configurational bias pattern. To increase computational performance the number of attempts depends on cluster population, being $n_{\rm dis} = 5$ when there is just one cluster and $n_{\rm dis} = 20$ when several exist.

Simulations are carried out in the NVT ensemble for three dimensions and in the NPT ensemble for two dimensions. In both cases, temperature is set equal to $T = 1/k$, where k is the Boltzmann constant. Pressure is fixed at 1 bar (NPT simulations) and packing density at $\varphi = 0.05$ (or equivalently number density $\rho_n = 0.0262$; NVT simulations). Due to the application of chain-connectivity-altering moves, dispersity in chain lengths is introduced. These vary uniformly with the minimum and maximum allowed lengths being set at six and 18 monomers, respectively. Selected simulations on polymers with longer lengths ($N_{av} = 24$), under the same conditions, revealed no appreciable difference in the phase behavior.

We start from a fully equilibrated athermal system of freely jointed chains of tangent hard spheres at low packing density [63] and activate the SW potential. As explained in detail in [57], this corresponds practically to instantaneous quenching with the attraction intensity adopting the role of an effective quench rate: the higher the value of ϵ, the higher the temperature difference. 2D polymer configurations are created by shrinking the original 3D systems until a film thickness of unit length is reached through a process that is described in [64]. By fixing all other parameters (N_{av}, N, T, P or V and dl) and the interaction intensity at $\epsilon = 1.2$, we systematically explore the effect of interaction range in the interval $\sigma_2 \in [1.10, \ldots, 2.00]$ in steps of 0.01 for 3D systems and in increments of 0.02 for 2D systems. As a first design step, a representative value of the well depth $\epsilon = 1.2$ is selected because it is (1) large enough to prevent entropy from overwhelming the internal energy advantage of specific crystals and (2) not so high that the simulations would become trapped in local energy minima, leading to glass formation instead of crystallization (see, for example, Fig. 5 in [57] on the phase behavior as a function of attraction intensity).

Equilibration of the systems is traced through a hierarchical, two-step evolution: (1) A single cluster is formed including all chains and their monomers. Quantification of this step is trivial by tracking the evolution of the number of formed clusters as the simulation evolves. Activation of cluster-based MC moves is a necessity especially for low values of σ_2 and/or high values of ϵ [57]. (2) The state or degree of order in the formed cluster becomes stable. This final step is quantified through the evolution of the degree of crystallinity, practically being equal to the sum of all order parameters for all reference crystals (see next section). To check reproducibility we have conducted additional simulations starting from different initial athermal configurations (but still under very dilute conditions) and with different seeds for the random number generators. For the whole range of σ_2 values studied, no appreciable difference is detected in the established morphologies between independent MC simulations.

D. Structural analysis of computer-generated system configurations

We employ the characteristic crystallographic element (CCE) norm [52,65] for the structural analysis of the computer-generated system configurations. In three dimensions we use the CCE norm to detect hexagonal close packed (HCP), face-centered cubic (FCC), simple hexagonal (HEX), and body-centered cubic (BCC) crystals as well as noncrystallographic fivefold (FIV) local symmetry. Regarding the 2D analysis, we compare against the triangular (TRI), square (SQU), and honeycomb (HON) crystals, as well as pentagonal (PEN) local symmetry. Every monomer in the system, in either two or three dimensions, is tested against all corresponding reference crystals as described above. Accordingly, a norm value μ_j^X is obtained for site j with respect to a reference crystal X. Here a threshold value of $\mu^c = 0.245$ is adopted, below which a site is considered as of X type. Furthermore, we can measure the order parameter, S^X, of a given X crystal as

$$S^X = \int_0^{\mu^c} P(\mu^X)\, d\mu^X \,, \tag{2}$$

where $P(\mu^X)$ is the probability distribution function over all monomers for a given configuration. In order to avoid considering the monomers that lie on the surface of the formed cluster the value of S^X is multiplied by $\frac{N}{N-N_{\rm surf}}$, where N is the number of sites in the simulation ($N = 1200$ in all simulations reported here) and $N_{\rm surf}$ is the number of monomers on the outer surface of the formed cluster. This is because in three dimensions under dilute conditions surface monomers lack a complete Voronoi environment and are thus characterized by high disorder (see also Fig. 9 and related discussion).

III. RESULTS

The activation of attractive potential dictating all intra- and interchain interactions leads to aggregation of the polymer chains and to the eventual formation of a single cluster, which may further crystallize depending on the values of interaction range and intensity. As stated earlier the selected value of $\epsilon = 1.2$ under the specific simulation conditions guarantees crystallization over glass formation as demonstrated in [57]. Once the single cluster containing all chains and monomers is formed, the CCE descriptor is employed to quantify the structural characteristics and the possible similarity to one of the reference crystals in two or three dimensions. Throughout the paper the following color convention is used: Blue, red, green, pink, and cyan correspond to HCP, FCC, FIV, HEX, and BCC similarity, respectively, for 3D systems; blue, red,

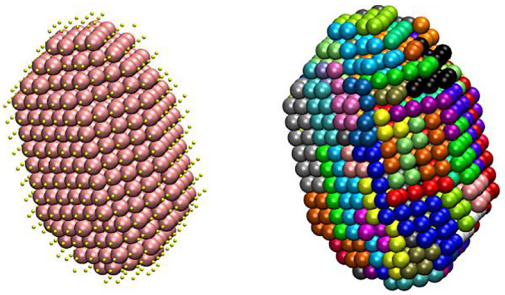

FIG. 2. Final stable polymer cluster as obtained from NVT simulations in three dimensions with interaction range set at $\sigma_2 = 1.51$. Left panel: Spheres are color coded according to their structural similarity: Blue, red, green, pink, and cyan correspond to HCP, FCC, FIV, HEX, and BCC similarity, respectively. Amorphous (AMO) sites are in yellow with reduced dimensions for clarity. Right panel: Spheres are colored according to their parent chain. Snapshots created with the VMD software [66].

green, and cyan correspond to TRI, SQU, PEN, and HON similarity, respectively, for 2D systems. Amorphous (or, more precisely, unidentified or "none of the above") sites (AMO) are shown in yellow (and with reduced dimensions in three dimensions for clarity).

An example of the formed single cluster of polymers at the end of the simulation and its structural identification through the CCE norm descriptor can be seen in Figs. 2 and 3, for 3D and 2D systems, respectively. On the left panel sites are colored according to their structural type, as quantified by the crystallographic analysis, and on the right panel monomers are colored according to the parent chain.

In the literature, simulation results are typically reported in reduced units of temperature ($T^* = (kT)/\epsilon$) and pressure ($P^* = (P\sigma_1^3)/\epsilon$), where T and P are the applied temperature and pressure and k is Boltzmann's constant. Here we deviate from the traditional approach and examine the important dependence on the attraction intensity, which, unlike T or P, is a material dependent, adjustable parameter, in accordance with

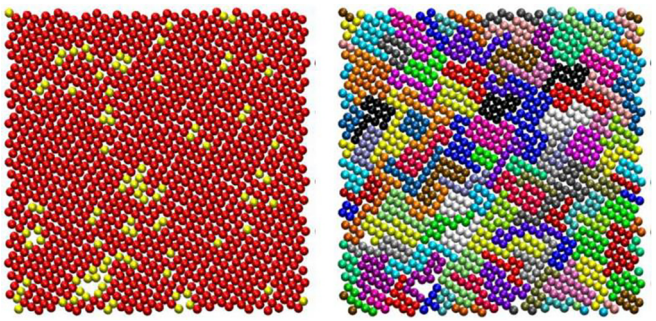

FIG. 3. Final stable polymer cluster as obtained from NPT simulations in two dimensions (polymer films of thickness equal to $\sigma_1 = 1$ with interaction range set at $\sigma_2 = 1.58$). Left panel: Spheres are color coded according to their structural similarity: Blue, red, green, and cyan correspond to TRI, SQU, PEN, and HON similarity, respectively. Amorphous (AMO) sites are in yellow. Right panel: Spheres are colored according to their parent chain. Snapshots created with the VMD software [66].

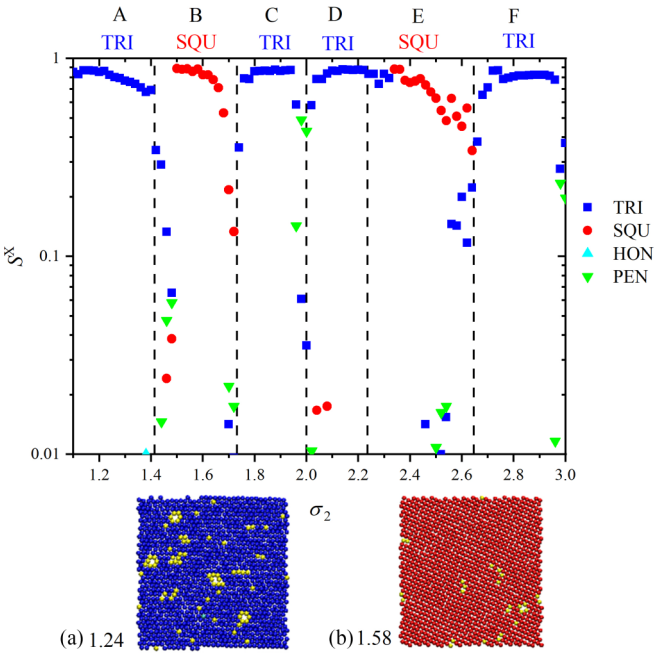

FIG. 4. Fraction of sites with a similarity to a given reference crystal or local symmetry X, S^X, as a function of the interaction range, σ_2, as obtained from MC simulations of attractive polymer chains in two dimensions (films of thickness equal to σ_1). Distinct regions, the thresholds, and the corresponding prevailing crystals, as predicted by the simple geometric neighbor model, are identified by the roman letters, the dashed vertical lines, and the color labels, respectively. Also shown are system configurations at the end of the simulation for selected values of the interaction range. Spheres are color coded according to their structural similarity: Blue, red, cyan, and green correspond to TRI, SQU, HON, and PEN similarity, respectively, as quantified by the CCE norm analysis [52]. Amorphous (AMO) sites colored in yellow. Snapshots created with the VMD software [66].

our goal to finely tune specific morphologies of hard colloidal polymers.

Figure 4 illustrates the strong effect, and hence the great tunability potential, of the interaction range σ_2: the order parameter for each reference crystal, S^X, is shown as a function of σ_2 for the 2D systems, together with the regions predicted by the simple geometric neighbor model and the expected prevailing crystals, based on energetic considerations only. Model predictions and simulation results are in excellent agreement, especially if we consider the simplicity of the model reported above. Furthermore, the proposed model predicts very accurately the values of the interaction range σ_2 at which polymorph transitions take place over the whole interaction range.

The immediate conclusion that can be drawn is that, for the reasonable well depth $\epsilon = 1.2$, entropy differences between polymorphs play a very subordinate role in the selection of a particular crystal type. This is in agreement with the known small differences in entropy among crystals of monomeric spheres [47–51], and also with recent quantitative estimates of differences in chain conformational entropy among crystals of polymers of hard spheres [59,67].

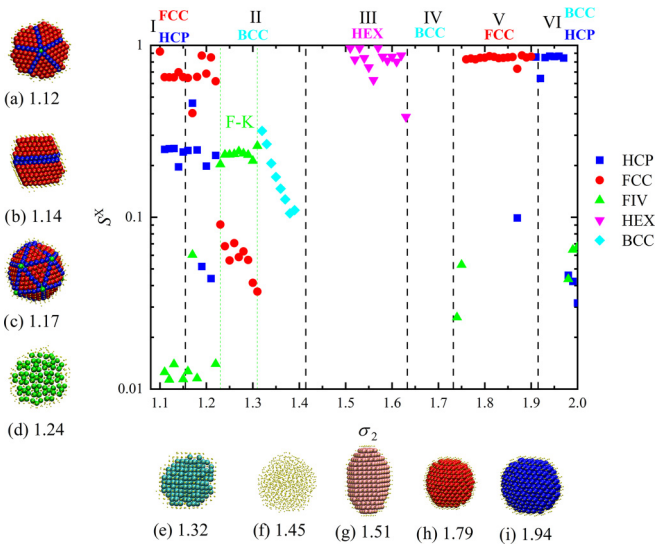

FIG. 5. Fraction of sites with a similarity to a given reference crystal as a function of the interaction range, as obtained from MC simulations on attractive polymer chains in bulk three dimensions. Outer surface monomers are excluded from the calculation of S^X. Distinct regions, the thresholds, and the corresponding prevailing crystals, as predicted by the geometric neighbor model, are identified by the roman numbers, the dashed vertical lines, and the color labels, respectively. Also shown are system configurations at the end of the simulation for selected values of the interaction range. Spheres are color coded according to their structural similarity: Blue, red, green, pink, and cyan correspond to HCP, FCC, FIV, HEX, and BCC similarity, respectively. Amorphous (AMO) sites are in yellow with reduced dimensions for clarity. The regime of the Frank-Kasper (F-K) phase, as established in simulations, is indicated by the vertical green dashed lines. Snapshots are created with VMD software [66] and are also available in Fig. 6, and for better visual inspection as 3D, interactive images in the Supplemental Material [68].

Figure 5 presents a similar phase diagram for the 3D systems, along with the predictions of the neighbor model, while Fig. 6 hosts representative snapshots at the end of the MC simulations. At short interaction range (Region I) a random hexagonal close packed (rHCP) crystal is observed. The rHCP morphology can have a unique stacking direction of fivefold-free HCP and FCC layers, or multiple stacking directions where the meeting (composition) planes at the crystal boundaries are fivefold-ridden. As the number of neighbors is the same between HCP and FCC no pure crystal prevails and, thus, the rHCP polymorph remains the final ordered morphology in Region I. The rHCP dominance, as gauged by simulations, extends into higher values of σ_2 than predicted by the neighbor model.

Interestingly, in the region between $1.21 \leqslant \sigma_2 \leqslant 1.30$ none of the crystals expected by the geometric model appear. The resulting structure is characterized by an abundance of fivefold sites and the absence of any appreciable population of sites with crystal similarity as captured by the CCE-norm descriptor. Close inspection of the established morphology, as hosted in Fig. 7, reveals that it corresponds to the σ variant of the Frank-Kasper (F-K) phase [69,70]. In the past, F-K phases have been reported in studies of self-organizing soft matter systems, including macromolecules, colloids, surfactants, and liquid crystals [71–81]. Red lines in Fig. 7 connect triangles "3" and squares "4" in the tiling of the sparsely populated layer of the F-K phase. The resulting tiling of $3^2.4.3.4$ is characteristic of the σ F-K phase.

The expected dominance of the imperfect BCC crystal sets in at higher values of σ_2, compared to the threshold predicted by the neighbor model. The transitions BCC (Region II) $\Leftrightarrow$ HEX (Region III) and HEX (Region III) $\Leftrightarrow$ BCC (Region IV) exist, as clearly captured by the data in Fig. 5. However, they are both accompanied by the presence of regions (called here "amorphous zones," denoted in the phase diagram as "AMO") of glassy, disordered behavior where no crystal traces are detected. The nature and origin of the two AMO zones, along the phase diagram, which is otherwise rich in distinct crystal morphologies, are open topics under study.

The FCC and HCP prevalence and the value of $\sigma_2 \approx 1.91$ at the transition agree very well with those expected from the number of neighbors in Regions V and VI. In fact, in Regions V and VI, we can observe the formation of perfect FCC and HCP crystals, in contrast to the behavior in Region I where the rHCP polymorph dominates. This trend can be explained rather trivially by the neighbor model: in Region I there is a tie in the number of neighbors ($m = 12$) for the HCP and FCC crystals, and hence in internal energy. The tiny entropic difference between FCC and HCP [67] is not sufficient to make FCC dominant in the MC simulation. However, in Regions V and VI the FCC and HCP crystals dominate by a difference of 2 and 10 neighbors, respectively, and are thus the energetically favored states. The high number of neighbors in these two regions ($m = 38$ and 50, respectively) also implies that monomers reside in a much deeper potential energy well, so that entropy plays a very minor role in selecting the stable polymorph, and in blurring the boundaries between phases.

In the present study we let the crystal be self-assembled in almost vacuum conditions, so it can spontaneously adjust its density and structure by obeying the tangency condition and the orientational and radial symmetry and by minimizing its free energy, chiefly by maximizing the number of neighbors within a shell of size σ_2. The complex phase diagram is primarily a consequence of this maximization. In order to interpret these observations, we plot in Fig. 8 the local number density, $\langle \rho_n \rangle$, the number of neighbors, $\langle m \rangle$, and the ratio of the accessible volume by the volume of the Voronoi cell, $\langle V_{ac}/V_{VC} \rangle$, as a function of interaction range. The brackets $\langle \quad \rangle$ denote here averaging over all monomers which have a fully developed Voronoi environment, i.e., that do not lie on the surface of the cluster, and over all system configurations in the final, stable part of the simulation trajectory. Local number density is calculated as the inverse of the Voronoi cell volume. The Voronoi tessellation, also a requirement for the crystallographic analysis, is done through the Voro++ software [82]. The regions observed in the MC simulations are identified in Fig. 8 by the different background colors and the corresponding labels. Well-defined crystals are characterized by a constant number of neighbors in particular ranges of σ_2, in agreement with the model predictions in Fig. 5, and by negative slope in the density curve: within the domain of a given polymorph, the crystal expands as σ_2 increases, while keeping the number of neighbors constant.

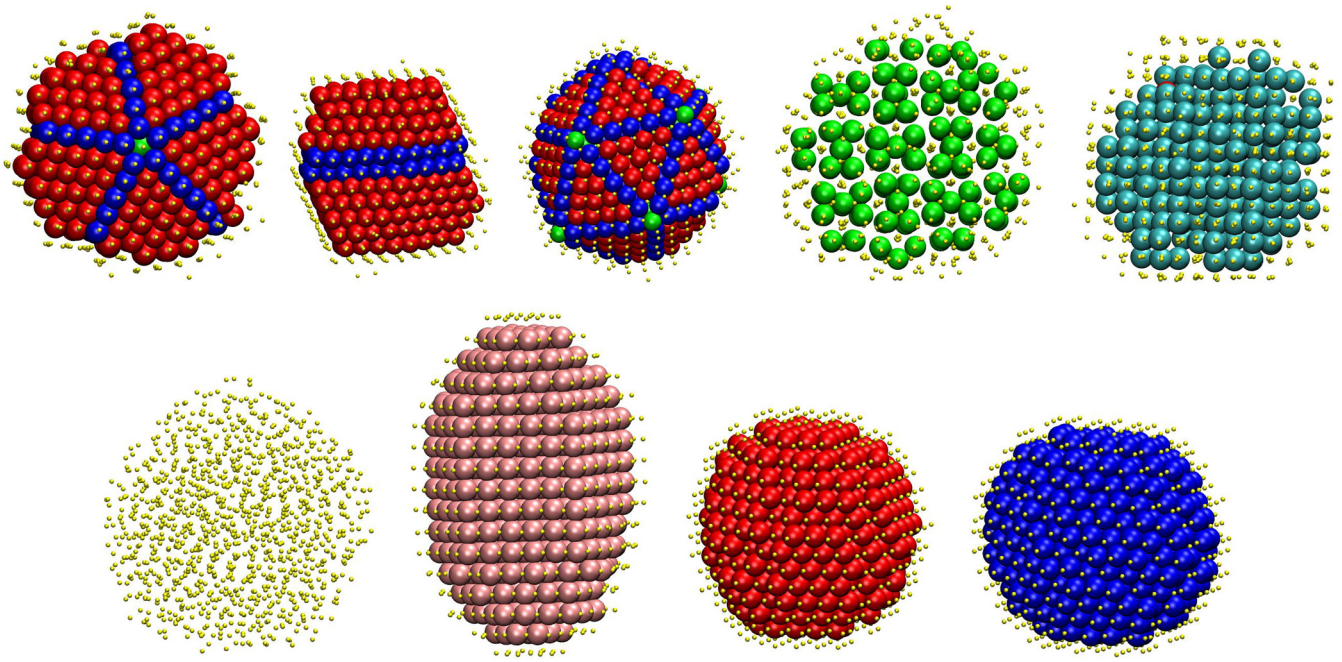

FIG. 6. Representative system configurations (bulk 3D) at the end of the Monte Carlo simulations with varied attraction range, σ_2. All chains have formed a single cluster of varied order and morphology. Top: $\sigma_2 = 1.12$ (random hexagonal close packed, rHCP), 1.14 (rHCP), 1.17 (rHCP), 1.24 (Frank-Kasper, F-K), and 1.32 (BCC); bottom: $\sigma_2 = 1.45$ (amorphous, AMO), 1.51 (HEX), 1.79 (FCC), and 1.94 (HCP). Labels in parentheses correspond to the established structures or morphologies. Spheres are color coded according to their structural similarity: Blue, red, green, pink, and cyan correspond to HCP, FCC, FIV, HEX, and BCC similarity, respectively. Amorphous (AMO) sites are colored in yellow with reduced dimensions for clarity. All clusters have the same number of monomers ($N = 1200$); their size may appear different because of the zoom level and the different viewing angle. Snapshots are created with the VMD software [66] and are also available for visual inspection as 3D, interactive images in the Supplemental Material [68].

In the crystalline regions where the number of neighbors remains constant, the energy is also strictly constant due to the flatness of the square well potential. Therefore, in

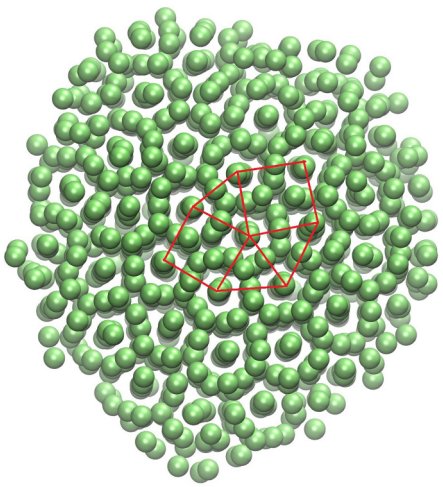

FIG. 7. System snapshot at the end of the MC simulation at $\sigma_2 = 1.23$ corresponding to the formation of the σ variant of the Frank-Kasper phase. Red lines are indicative of the tiling pattern of squares ("4") and triangles ("3") applied on the sparsely populated layer of spheres corresponding to the $3^2.4.3.4$ format. The lime color used here is not to be confused with the green to indicate FIV similarity through the CCE-norm description.

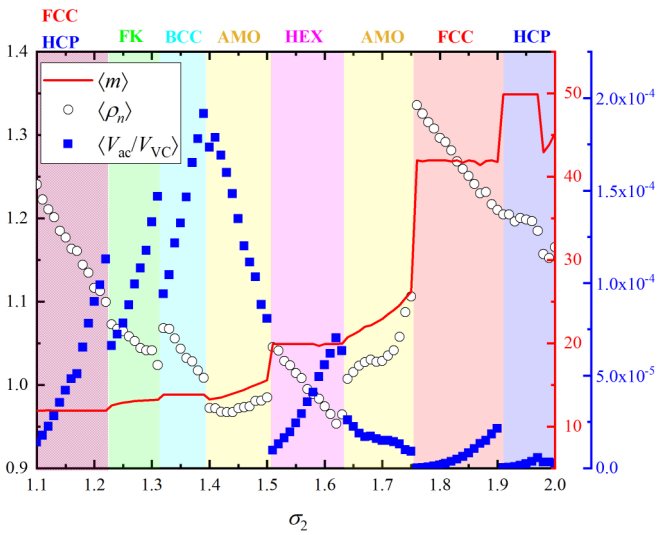

FIG. 8. Local number density $\langle \rho_n \rangle$ (left y axis, white circles), number of neighbors $\langle m \rangle$ (right y axis, red line), and ratio of accessible volume divided by the total volume of the Voronoi cell $\langle V_{ac}/V_{VC} \rangle$ (right y axis, blue squares) inside a shell of radius σ_2 as a function of σ_2. $\langle \ \ \rangle$ corresponds to average over all sites with a fully developed Voronoi environment (i.e., surface monomers of the cluster are excluded from the analysis) and all snapshots that belong to the equilibrated part of the trajectory. Background colors correspond to the dominant (crystal, F-K, or amorphous) phase as observed in the MC simulations.

these regions minimization of free energy is tantamount to maximization of entropy, most of which is of translational origin [47–51] and, ignoring for simplicity the shape of the local environment, is proportional to the volume accessible to the monomers. In parallel, an expansion of the Voronoi cell is also taking place, driven by entropy. This expansion is reflected in a higher accessible volume (V_{ac}), which eventually increases the translational entropy of the monomers. The accessible volume can be estimated through MC integration, considering that V_{ac} is effectively the fraction of the Voronoi cell volume (V_{VC}) where a spherical monomer can be placed without overlapping with the walls of the enclosing polyhedron. So long as the number of neighbors remains constant, the crystal expands with increasing σ_2 primarily because of the increase in translational entropy of the chain monomers. Chain conformational entropy changes only very weakly with σ_2 and is thus not the driving force for crystal expansion with σ_2. Figure 8 shows clearly that the accessible volume increases in the crystal regions, while in the AMO zones, where amorphous behavior is observed, it tends to shrink.

Transitions between well-defined crystals, for example, the FCC ⇔ HCP transition, are marked by a jump in the number of neighbors and a moderate change in the (still negative) density slope. The behavior changes drastically in the transition between well-defined crystals and the AMO zones where disorder prevails. There, the amorphous cluster contracts and the number of neighbors increases in a smooth, rather than stepwise, pattern. This behavior is identical for both AMO zones, which surround the domain of HEX-ordered morphologies. Negative density slopes are a rather straightforward consequence of entropic pressure: as long as the sites remain within the interaction range, increasing the cell volume leads to larger translational entropy. The expansion is then energetically neutral and entropically favorable, so that the crystal expands. As σ_2 grows beyond specific limits, the number of neighbors and thus its stability increases through a transition to another polymorph, mostly driven by internal energy.

The left panel of Fig. 9 (scattered white circles) shows the percentage of the monomers lying on the external surface of the formed cluster as a function of interaction range, σ_2. Quite small deviations occur within the whole range, with around two-thirds of the sites having a fully developed Voronoi cell. Between the formed crystals the HEX one shows the highest surface to volume ratio. In general, the more compact and the more spherical the cluster the fewer the sites on the surface. Two distinct trends can be further observed: the number of surface atoms increases as a function of σ_2 for the Frank-Kasper phase but decreases monotonically in the amorphous zones. The right panel of Fig. 9 (red solid line) shows the dependence of the percentage difference of the number of neighbors, $100\Delta m/m$, on σ_2. Δm is defined here as a the number of neighbors, as predicted by the proposed geometric model, minus the number of neighbors as calculated in the computer-generated system configurations including all snapshots in the equilibrated part of the MC trajectory. Very good to excellent agreement is observed in all regions where the crystal formed in the MC simulations coincides with the dominant one as predicted by the geometric model. Large deviations correspond to the two amorphous zones, an expected trend as these regions are bare of any crystal order. These are

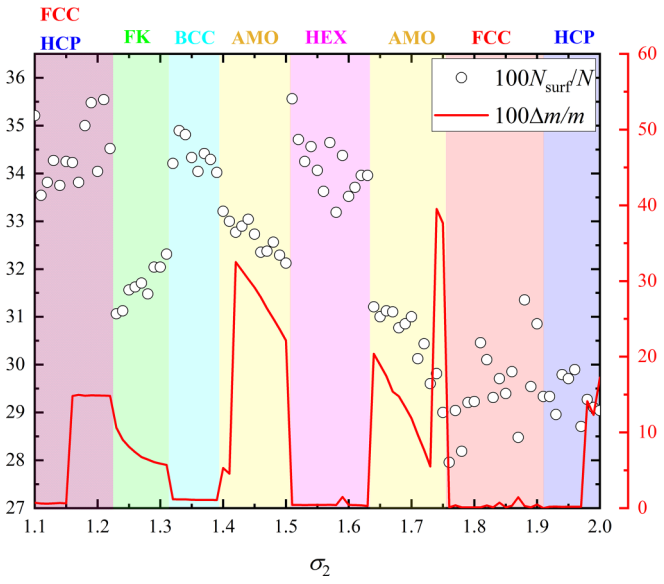

FIG. 9. Percentage of monomers lying on the external surface of the formed cluster, $100N_{surf}/N$ (left y axis, scattered points) and percentage difference in the number of neighbors $100\Delta m/m$ (right y axis, red line) as a function of σ_2. Δm is defined as the number of neighbors as predicted by the geometric model, m, minus the number of neighbors as calculated in the computer-generated system configurations. Background colors correspond to the dominant (crystal, F-K, or amorphous) phase as observed in the MC simulations.

further accompanied by abrupt changes marking the AMO ⇔ HEX and HEX ⇔ AMO transitions. In the early regime a sharp discrepancy is observed as the expected BCC crystal, according to the model, is not encountered in the computer simulations and instead rHCP morphologies of mixed FCC and HCP character are formed. In parallel, the difference in the number of neighbors adopts the lowest values in the HEX- and FCC-dominated regions. It should be further noted that for the whole interaction range studied here no negative values in Δm are observed. If such values existed it would mean that the MC simulations generate a stable crystal which is denser and thus different from the reference ones incorporated in the geometric neighbor model.

IV. CONCLUSIONS

The Digital Alchemy proposed by Anders *et al.* [1] and recent important advances in synthesis and characterization show how the use of building blocks of low dimensionality can lead to the design of tailored colloidal polymers and molecules by controlling chain stiffness and molecular architecture [15,17,19,20]. The present work demonstrates, at a fundamental level and utilizing a highly idealized model, how fine tuning a single interaction parameter can be used to obtain a rich assortment of target crystal structures in bulk 3D and ultrathin 2D films of hard colloidal chains of attractive monomers. Towards this, first, we propose a simple geometric model, based on the cumulative number of neighbors, to predict the dominant crystal as a function of attraction range. Then, we embark on Monte Carlo simulations, using the square well potential to equilibrate and

successively identify the computer-generated polymer clusters. The flatness of the square well potential makes it ideal to compare the computer-generated structures against the reference crystals predicted by the geometric model. By tuning the attraction range a wealth of well-defined ordered structures is observed including hexagonal closed packed, face-centered cubic, simple hexagonal, and body-centered cubic crystals in three dimensions and triangular and cubic crystals in two. The 3D ordered morphologies are further accompanied by Frank-Kasper phases of the σ variant. Interestingly, the expected transitions between the HEX and BCC crystals are suppressed by the presence of amorphous zones where no traces of crystallization can be detected. In spite of its simplicity the proposed geometrical model, as demonstrated by the Monte Carlo simulations, is able to predict the dominant phases and the corresponding transitions with high accuracy, especially in two dimensions.

Current efforts focus on gauging the corresponding phase behavior of semiflexible polymer chains under the same simulation conditions in the bulk (3D) and in extremely confined thin films (2D).

The data corresponding to the crystallographic analysis applied on the final configurations at the end of the MC simulations are openly available [83].

ACKNOWLEDGMENTS

M.H. deeply appreciates the kind hospitality of the COMSE group (NTUA, Athens, Greece) during his stay. The authors acknowledge support through Projects No. PID2021-127533NB-I00 and No. RTI2018-097338-B-I00 of MICINN/FEDER (Ministerio de Ciencia e Innovación, Fondo Europeo de Desarrollo Regional). M.H. and D.M.F. acknowledge financial support through the Programa Propio UPM Santander of Universidad Politécnica de Madrid (UPM) and Santander Bank. The authors gratefully acknowledge the UPM for providing computing resources on the Magerit supercomputer through Projects No. r553, No. r727, No. s341, No. t736, and No. u242.

[1] G. van Anders, D. Klotsa, A. S. Karas, P. M. Dodd, and S. C. Glotzer, Digital alchemy for materials design: Colloids and beyond, ACS Nano **9**, 9542 (2015).

[2] B. Li, S. Zhang, J. S. Andre, and Z. Chen, Relaxation behavior of polymer thin films: Effects of free surface, buried interface, and geometrical confinement, Prog. Polym. Sci. **120**, 101431 (2021).

[3] P. F. Damasceno, M. Engel, and S. C. Glotzer, Predictive self-assembly of polyhedra into complex structures, Science **337**, 453 (2012).

[4] F. H. Stillinger, R. L. Kornegay, and E. A. Dimarzio, Systematic approach to explanation of rigid disk phase transition, J. Chem. Phys. **40**, 1564 (1964).

[5] E. L. Hinrichsen, J. Feder, and T. Jossang, Random packing of disks in two dimensions, Phys. Rev. A **41**, 4199 (1990).

[6] W. M. Visscher and M. Bosterl, Random packing of equal and unequal spheres in two and three dimensions, Nature (London) **239**, 504 (1972).

[7] S. Meyer, C. M. Song, Y. L. Jin, K. Wang, and H. A. Makse, Jamming in two-dimensional packings, Physica A **389**, 5137 (2010).

[8] Z. Gong, T. Hueckel, G. R. Yi, and S. Sacanna, Patchy particles made by colloidal fusion, Nature (London) **550**, 234 (2017).

[9] C. L. Kennedy, D. Sayasilpi, P. Schall, and J. M. Meijer, Self-assembly of colloidal cube superstructures with critical Casimir attractions, J. Phys.: Condens. Matter **34**, 214005 (2022).

[10] A. Kuijk, A. van Blaaderen, and A. Imhof, Synthesis of monodisperse, rodlike silica colloids with tunable aspect ratio, J. Am. Chem. Soc. **133**, 2346 (2011).

[11] S. Sacanna, W. T. M. Irvine, P. M. Chaikin, and D. J. Pine, Lock and key colloids, Nature (London) **464**, 575 (2010).

[12] S. Sacanna, M. Korpics, K. Rodriguez, L. Colon-Melendez, S. H. Kim, D. J. Pine, and G. R. Yi, Shaping colloids for self-assembly, Nat. Commun. **4**, 1688 (2013).

[13] Y. N. Xia, Y. J. Xiong, B. Lim, and S. E. Skrabalak, Shape-controlled synthesis of metal nanocrystals: Simple chemistry meets complex physics? Angew. Chem. Int. Ed. **48**, 60 (2009).

[14] G. Reiter and J. Sommer, *Polymer Crystallization: Obervations, Concepts and Interpretations* (Springer, Berlin, 2008).

[15] X. L. Fan and A. Walther, 1D Colloidal chains: Recent progress from formation to emergent properties and applications, Chem. Soc. Rev. **51**, 4023 (2022).

[16] F. Li, D. P. Josephson, and A. Stein, Colloidal assembly: The road from particles to colloidal molecules and crystals, Angew. Chem. Int. Ed. **50**, 360 (2011).

[17] I. Chakraborty, D. J. G. Pearce, R. W. Verweij, S. C. Matysik, L. Giomi, and D. J. Kraft, Self-assembly dynamics of reconfigurable colloidal molecules, ACS Nano **16**, 2471 (2022).

[18] L. J. Huil, N. Pinna, K. Char, and J. Pyun, Colloidal polymers from inorganic nanoparticle monomers, Prog. Polym. Sci. **40**, 85 (2015).

[19] W. Y. Li, H. Palis, R. Merindol, J. Majimel, S. Ravaine, and E. Duguet, Colloidal molecules and patchy particles: Complementary concepts, synthesis and self-assembly, Chem. Soc. Rev. **49**, 1955 (2020).

[20] F. Martinez-Pedrero, A. Gonzalez-Banciella, A. Camino, A. Mateos-Maroto, F. Ortega, R. G. Rubio, I. Pagonabarraga, and C. Calero, Static and dynamic self-assembly of pearl-like-chains of magnetic colloids confined at fluid interfaces, Small **17**, 2101188 (2021).

[21] S. Stuij, J. M. van Doorn, T. Kodger, J. Sprakel, C. Coulais, and P. Schall, Stochastic buckling of self-assembled colloidal structures, Phys. Rev. Res. **1**, 023033 (2019).

[22] R. W. Verweij, P. G. Moerman, N. E. G. Ligthart, L. P. P. Huijnen, J. Groenewold, W. K. Kegel, A. van Blaaderen, and D. J. Kraft, Flexibility-induced effects in the Brownian motion of colloidal trimers, Phys. Rev. Res. **2**, 033136 (2020).

[23] H. R. Vutukuri, A. F. Demirors, B. Peng, P. D. J. van Oostrum, A. Imhof, and A. van Blaaderen, Colloidal analogues of charged and uncharged polymer chains with tunable stiffness, Angew. Chem. Int. Ed. **51**, 11249 (2012).

[24] J. D. Dietz and R. S. Hoy, Two-stage athermal solidification of semiflexible polymers and fibers, Soft Matter **16**, 6206 (2020).

[25] N. A. Mahynski, S. K. Kumar, and A. Z. Panagiotopoulos, Relative stability of the FCC and HCP polymorphs with interacting polymers, Soft Matter **11**, 280 (2015).
[26] N. A. Mahynski, A. Z. Panagiotopoulos, D. Meng, and S. K. Kumar, Stabilizing colloidal crystals by leveraging void distributions, Nat. Commun. **5**, 4472 (2014).
[27] T. Shakirov, Crystallisation in melts of short, semi-flexible hard-sphere polymer chains: The role of the non-bonded interaction range, Entropy **21**, 856 (2019).
[28] R. W. Verweij, P. G. Moerman, L. P. P. Huijnen, N. E. G. Ligthart, I. Chakraborty, J. Groenewold, W. K. Kegel, A. van Blaaderen, and D. J. Kraft, Conformations and diffusion of flexibly linked colloidal chains, J. Phys. Mater. **4**, 035002 (2021).
[29] N. C. Karayiannis, K. Foteinopoulou, and M. Laso, The role of bond tangency and bond gap in hard sphere crystallization of chains, Soft Matter **11**, 1688 (2015).
[30] R. Ni and M. Dijkstra, Effect of bond length fluctuations on crystal nucleation of hard bead chains, Soft Matter **9**, 365 (2013).
[31] D. A. Young and B. J. Alder, Studies in molecular dynamics. XVII. Phase diagrams for step potentials in two and three dimensions, J. Chem. Phys. **70**, 473 (1979).
[32] D. A. Young and B. J. Alder, Studies in molecular-dynamics. SVIII. The square-well phase diagram, J. Chem. Phys. **73**, 2430 (1980).
[33] J. C. Armas-Pérez, J. Quintana-H, G. A. Chapela, E. Velasco, and G. Navascués, Phase diagram of a square-well model in two dimensions, J. Chem. Phys. **140**, 064503 (2014).
[34] B. C. Attwood and C. K. Hall, Global phase diagram for monomer/dimer mixtures, Fluid Phase Equilib. **204**, 85 (2003).
[35] S. Babu, J. C. Gimel, and T. Nicolai, Crystallization and dynamical arrest of attractive hard spheres, J. Chem. Phys. **130**, 064504 (2009).
[36] T. K. Haxton, L. O. Hedges, and S. Whitelam, Crystallization and arrest mechanisms of model colloids, Soft Matter **11**, 9307 (2015).
[37] A. Prabhu, S. B. Babu, J. S. Dolado, and J. C. Gimel, Brownian cluster dynamics with short range patchy interactions: Its application to polymers and step-growth polymerization, J. Chem. Phys. **141**, 024904 (2014).
[38] W. Rżysko, A. Patrykiejew, S. Sokołowski, and O. Pizio, Phase behavior of a two-dimensional and confined in slitlike pores square-shoulder, square-well fluid, J. Chem. Phys. **132**, 164702 (2010).
[39] J. Serrano-Illán, G. Navascués, and E. Velasco, Noncompact crystalline solids in the square-well potential, Phys. Rev. E **73**, 011110 (2006).
[40] E. M. Sevick and P. A. Monson, Cluster integrals for square-well particles—Application to percolation, J. Chem. Phys. **94**, 3070 (1991).
[41] S. Takada and H. Hayakawa, Rheology of dilute cohesive granular gases, Phys. Rev. E **97**, 042902 (2018).
[42] S. Schnabel, M. Bachmann, and W. Janke, Elastic Lennard-Jones polymers meet clusters: Differences and similarities, J. Chem. Phys. **131**, 124904 (2009).
[43] S. Schnabel, W. Janke, and M. Bachmann, Advanced multicanonical Monte Carlo methods for efficient simulations of nucleation processes of polymers, J. Comput. Phys. **230**, 4454 (2011).
[44] S. Schnabel, T. Vogel, M. Bachmann, and W. Janke, Surface effects in the crystallization process of elastic flexible polymers, Chem. Phys. Lett. **476**, 201 (2009).
[45] M. P. Taylor, W. Paul, and K. Binder, Phase transitions of a single polymer chain: A Wang–Landau simulation study, J. Chem. Phys. **131**, 114907 (2009).
[46] J. Zierenberg, M. Marenz, and W. Janke, Dilute semiflexible polymers with attraction: Collapse, folding and aggregation, Polymers **8**, 333 (2016).
[47] L. V. Woodcock, Entropy difference between the face-centred cubic and hexagonal close-packed crystal structures, Nature (London) **385**, 141 (1997).
[48] J. M. Polson, E. Trizac, S. Pronk, and D. Frenkel, Finite-size corrections to the free energies of crystalline solids, J. Chem. Phys. **112**, 5339 (2000).
[49] P. G. Bolhuis, D. Frenkel, S. C. Mau, and D. A. Huse, Entropy difference between crystal phases, Nature (London) **388**, 235 (1997).
[50] S. C. Mau and D. A. Huse, Stacking entropy of hard-sphere crystals, Phys. Rev. E **59**, 4396 (1999).
[51] E. G. Noya and N. G. Almarza, Entropy of hard spheres in the close-packing limit, Mol. Phys. **113**, 1061 (2015).
[52] P. M. Ramos, M. Herranz, K. Foteinopoulou, N. C. Karayiannis, and M. Laso, Identification of local structure in 2-D and 3-D atomic systems through crystallographic analysis, Crystals **10**, 1008 (2020).
[53] M. Herranz, D. Martínez-Fernández, P. M. Ramos, K. Foteinopoulou, N. C. Karayiannis, and M. Laso, Simu-D: A simulator-descriptor suite for polymer-based systems under extreme conditions, Intl. J. Mol. Sci. **22**, 12464 (2021).
[54] N. C. Karayiannis, V. G. Mavrantzas, and D. N. Theodorou, A Novel Monte Carlo Scheme for the Rapid Equilibration of Atomistic Model Polymer Systems of Precisely Defined Molecular Architecture, Phys. Rev. Lett. **88**, 105503 (2002).
[55] N. C. Karayiannis and M. Laso, Monte Carlo scheme for generation and relaxation of dense and nearly jammed random structures of freely jointed hard-sphere chains, Macromolecules **41**, 1537 (2008).
[56] P. M. Ramos, N. C. Karayiannis, and M. Laso, Off-lattice simulation algorithms for athermal chain molecules under extreme confinement, J. Comput. Phys. **375**, 918 (2018).
[57] M. Herranz, M. Santiago, K. Foteinopoulou, N. C. Karayiannis, and M. Laso, Crystal, fivefold and glass formation in clusters of polymers interacting with the square well potential, Polymers **12**, 1111 (2020).
[58] P. M. Ramos, M. Herranz, K. Foteinopoulou, N. C. Karayiannis, and M. Laso, Entropy-driven heterogeneous crystallization of hard-sphere chains under unidimensional confinement, Polymers **13**, 1352 (2021).
[59] M. Herranz, K. Foteinopoulou, N. C. Karayiannis, and M. Laso, Polymorphism and perfection in crystallization of hard sphere polymers, Polymers **14**, 4435 (2022).
[60] D. Martínez-Fernández, M. Herranz, K. Foteinopoulou, N. C. Karayiannis, and M. Laso, Local and global order in dense packings of semi-flexible polymers of hard spheres, Polymers **15**, 551 (2023).
[61] M. Ester, H.-P. Kriegel, J. Sander, and X. Xu, A density-based algorithm for discovering clusters in large spatial databases with noise, in *Proc. 2nd Intl. Conf. on Knowledge Discovery and Data*

Mining (KDD-96), edited by E. Simoudis, J. Han, and U. M. Fayyad (AAAI Press, Cambridge, MA, 1996), pp. 226–231.

[62] E. Schubert, J. Sander, M. Ester, H. P. Kriegel, and X. W. Xu, DBSCAN revisited, revisited: Why and how you should (still) use DBSCAN, ACM Trans. Database Syst. **42**, 1 (2017).

[63] N. C. Karayiannis, K. Foteinopoulou, and M. Laso, The structure of random packings of freely jointed chains of tangent hard spheres, J. Chem. Phys. **130**, 164908 (2009).

[64] C. Pedrosa, D. Martínez-Fernández, M. Herranz, K. Foteinopoulou, N. C. Karayiannis, and M. Laso, Densest packing of flexible polymers in 2D films, J. Chem. Phys. **158**, 164502 (2023).

[65] N. C. Karayiannis, K. Foteinopoulou, and M. Laso, The characteristic crystallographic element norm: A descriptor of local structure in atomistic and particulate systems, J. Chem. Phys. **130**, 074704 (2009).

[66] W. Humphrey, A. Dalke, and K. Schulten, VMD: Visual molecular dynamics, J. Mol. Graph. **14**, 33 (1996).

[67] M. Herranz, J. Benito, K. Foteinopoulou, N. C. Karayiannis, and M. Laso, Polymorph stability and free energy of crystallization of freely-jointed polymers of hard spheres, Polymers **15**, 1335 (2023).

[68] See Supplemental Material at http://link.aps.org/supplemental/10.1103/PhysRevE.107.064605 for interactive, 3D images for selected system configurations.

[69] F. C. Frank and J. S. Kasper, Complex alloy structures regarded as sphere packings. I. Definitions and basic principles, Acta Crystallogr. **11**, 184 (1958).

[70] F. C. Frank and J. S. Kasper, Complex alloy structures regarded as sphere packing. II. Analysis and classification of representative structures, Acta Crystallogr. **12**, 483 (1959).

[71] M. J. Huang, K. Yue, J. Wang, C. H. Hsu, L. G. Wang, and S. Z. D. Cheng, Frank-Kasper and related quasicrystal spherical phases in macromolecules, Sci. China Chem. **61**, 33 (2018).

[72] G. Ungar and X. B. Zeng, Frank-Kasper, quasicrystalline and related phases in liquid crystals, Soft Matter **1**, 95 (2005).

[73] M. J. Huang, C. H. Hsu, J. Wang, S. Mei, X. H. Dong, Y. W. Li, M. X. Li, H. Liu, W. Zhang, T. Z. Aida *et al.*, Selective assemblies of giant tetrahedra via precisely controlled positional interactions, Science **348**, 424 (2015).

[74] A. B. Chang and F. S. Bates, Impact of architectural asymmetry on Frank-Kasper phase formation in block polymer melts, ACS Nano **14**, 11463 (2020).

[75] Z. B. Su, R. M. Zhang, X. Y. Yan, Q. Y. Guo, J. H. Huang, W. P. Shan, Y. C. Liu, T. Liu, M. J. Huang, and S. Z. D. Cheng, The role of architectural engineering in macromolecular self-assemblies via non-covalent interactions: A molecular LEGO approach, Prog. Polym. Sci. **103**, 101230 (2020).

[76] L. Han and S. N. Che, Anionic surfactant templated mesoporous silicas (AMSs), Chem. Soc. Rev. **42**, 3740 (2013).

[77] S. D. Hudson, H. T. Jung, V. Percec, W. D. Cho, G. Johansson, G. Ungar, and V. S. K. Balagurusamy, Direct visualization of individual cylindrical and spherical supramolecular dendrimers, Science **278**, 449 (1997).

[78] E. V. Shevchenko, D. V. Talapin, N. A. Kotov, S. O'Brien, and C. B. Murray, Structural diversity in binary nanoparticle superlattices, Nature (London) **439**, 55 (2006).

[79] H. Takagi and K. Yamamoto, Phase boundary of Frank-Kasper sigma phase in phase diagrams of binary mixtures of block copolymers and homopolymers, Macromolecules **52**, 2007 (2019).

[80] M. Z. Chen, Y. T. Huang, C. Y. Chen, and H. L. Chen, Accessing the Frank-Kasper sigma phase of block copolymer with small conformational asymmetry via selective solvent solubilization in the micellar corona, Macromolecules **55**, 10812 (2022).

[81] B. A. Lindquist, R. B. Jadrich, W. D. Pineros, and T. M. Truskett, Inverse design of self-assembling Frank-Kasper phases and insights into emergent quasicrystals, J. Phys. Chem. B **122**, 5547 (2018).

[82] C. H. Rycroft, VORO++: A three-dimensional Voronoi cell library in C + +, Chaos **19**, 041111 (2009).

[83] https://zenodo.org/record/7985451.